Bachelorarbeit im Fach Physik

Sensitivity Studies for the Model Unspecific Search in CMS (MUSiC) at $\sqrt{s}$=13 TeV

von

Arne Stroucken

vorgelegt der
Fakultät für Mathematik, Informatik und Naturwissenschaften der RWTH Aachen

im August 2016

angefertigt am

III. Physikalischen Institut A

bei

Prof. Dr. Thomas Hebbeker

Eidesstattliche Versicherung

Name, Vorname

Matrikelnummer (freiwillige Angabe)

Ich versichere hiermit an Eides Statt, dass ich die vorliegende Arbeit/Bachelorarbeit/ Masterarbeit* mit dem Titel

selbständig und ohne unzulässige fremde Hilfe erbracht habe. Ich habe keine anderen als die angegebenen Quellen und Hilfsmittel benutzt. Für den Fall, dass die Arbeit zusätzlich auf einem Datenträger eingereicht wird, erkläre ich, dass die schriftliche und die elektronische Form vollständig übereinstimmen. Die Arbeit hat in gleicher oder ähnlicher Form noch keiner Prüfungsbehörde vorgelegen.

Ort, Datum

Unterschrift

*Nichtzutreffendes bitte streichen

Belehrung:

§ 156 StGB: Falsche Versicherung an Eides Statt

Wer vor einer zur Abnahme einer Versicherung an Eides Statt zuständigen Behörde eine solche Versicherung falsch abgibt oder unter Berufung auf eine solche Versicherung falsch aussagt, wird mit Freiheitsstrafe bis zu drei Jahren oder mit Geldstrafe bestraft.

§ 161 StGB: Fahrlässiger Falscheid; fahrlässige falsche Versicherung an Eides Statt

(1) Wenn eine der in den §§ 154 bis 156 bezeichneten Handlungen aus Fahrlässigkeit begangen worden ist, so tritt Freiheitsstrafe bis zu einem Jahr oder Geldstrafe ein.

(2) Straflosigkeit tritt ein, wenn der Täter die falsche Angabe rechtzeitig berichtigt. Die Vorschriften des § 158 Abs. 2 und 3 gelten entsprechend.

Die vorstehende Belehrung habe ich zur Kenntnis genommen:

Ort, Datum

Unterschrift

Abstract

The Model Unspecific Search in CMS (MUSiC) is an approach to analyse the data taken with the CMS detector at the Large Hadron Collider at CERN. This thesis uses the MUSiC code developed for the analysis of the measurements performed at a centre of mass energy of 13 TeV. In contrast to dedicated analyses, MUSiC does not pursue a search strategy which is optimised for a certain theory prediction beyond the Standard Model of particle physics.
One of the final outcomes of the MUSiC analysis is a global comparison between the deviations between measurement and Standard Model Monte Carlo simulations and the statistically expected deviations expected from the Standard Model only hypothesis, the $\tilde{p}$-distribution. The aim of this thesis is to conduct a sensitivity study by investigating the effects an injected signal instead of observed data has on the distribution. The examined signal samples originate from Monte Carlo simulations on the basis of an R-parity-violating Supersymmetry model with a specific choice of supersymmetrical couplings constants. The effects of scenarios with different tau-sneutrino masses are considered. It appears that MUSiC is principally sensitive to the model in question, but the extent of deviation depends strongly on the choice of tau-sneutrino masses as parameters. The achieved sensitivity is compared to the sensitivity of the dedicated analysis [9] with the result that the sensitivities of both approaches are similar for the considered model.

Contents

1 The Standard Model of Particle Physics

1.1 Introduction

The Standard Model (SM) is the currently most widely spread theory in particle physics. Describing the elementary particles and the most important interactions between them, it is in good accordance with the experimental data taken at modern particle accelerators [1]. However, there are also some shortcomings and open questions which motivate research activities like the analysis of the CMS-data with a model unspecific approach considered in this thesis.
This chapter gives a brief summary of the Standard Model and a discussion of its shortcomings and open questions.

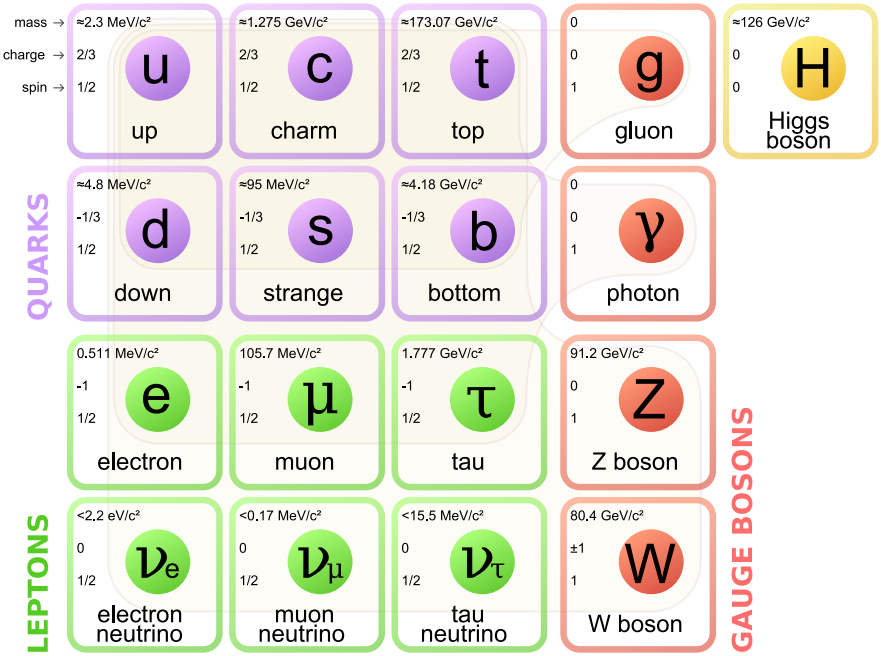

Figure 1: An overview over all SM-particles including their properties mass, charge and spin. [2].

1.2 Elementary Particles

According to the Standard Model, all physical processes can be described by seventeen elementary (meaning not further divisible) particles with different properties and dynamics (an overview is provided in figure 1). It contains five particles with integer spin called bosons, and twelve particles with half integer spin known as fermions. For each particle an antiparticle as counterpart with opposite sign in all charge-like quantum numbers exists. However, this does not increase the total number of particles by a factor of two, since some of the particles are their own antiparticles (e.g. the photon). For neutrinos it is not yet known whether particle and antiparticle coincide. In this case one would speak of

Majorana-fermions.
What we usually refer to as matter, turns out to be build up of fermions, whereas the role of bosons is to mediate the forces between those matter-particles.
Fermions are further divided into quarks and leptons, whereby charged (e, μ, τ) and uncharged (neutrinos ν_e, ν_μ, ν_τ) leptons exist. The difference between quarks and leptons is that only the former interact strongly. All fermions can be organised in three generations as portrayed in figure 1.
Bosons on the other hand are further divided into gauge and scalar bosons (spin 1, respectively 0 [1]). While there is only one scalar boson in the Standard Model (the Higgs Boson which gives the particles mass), there are four types of gauge bosons: gluons mediating the strong force, the photon mediating the electromagnetic force and W- and Z-boson mediating the weak force.

1.3 Shortcomings and Open Questions

Since the Standard Model does not include gravity as elementary force, it cannot be regarded as a complete theory, but even the described interactions (electromagnetic, strong, weak) are not unified to a single one like one might possibly desire. Instead, only electromagnetic and weak interaction are combined to the so-called electroweak force, whereas the strong interaction remains completely ununified.
Another deficit is that the predictive power of the Standard Model is reduced by the fact that it still contains a certain number of free parameters (at least 19 according to [4]). Even though meanwhile all parameters relevant for collider physics have been determined in experiments, a theory with less degrees of freedom is to prefer because of its more precise way of description.
Moreover, the Standard Model is in contradiction to recent observations of neutrino-oscillations: for the existence of those, at least one non vanishing neutrino mass is necessary [5], but the model presumes all masses of neutrinos to be zero.
It additionally fails to explain the observed asymmetry between matter and antimatter in the universe as well as the existence of dark energy discovered with astronomical methods. Furthermore it does not provide a proper candidate for a weakly interacting massive particle (WIMP) to explain the indirect detection of dark matter.
In the current version of the Standard Model the hierarchy problem dealing with the mass of the Higgs-Boson likewise remains unsolved.

1.4 New Physics

The depicted difficulties should be motivation enough to initiate a search for physics beyond the Standard Model - usually referred to as “BSM“ or “new physics“. There are diverse approaches dealing with this issue; R-parity violating supersymmetry is one of them.

[1] Note that this is in accordance to the definition of bosons as particles with integer spins.

2 Supersymmetry

2.1 General Idea

While there are several types of supersymmetrical theories (e.g. Minimal Supersymmetric Standard Model (MSSM), Next to Minimal Supersymmetric Standard Model (NMSSM); R-Parity-conserving, R-parity-violating), the general and most basic concept of supersymmetry (SUSY) stays the same for all of them: the particle content of the Standard Model is extended by the introduction of so-called superpartners with differing spin.
For each fermion the existence of a corresponding boson is postulated and vice versa. This procedure is illustrated in figure 2. To create SUSY as a self-consistent theory the introduction of at least one further Higgs-doublet (with a corresponding superpartner) is additionally required.

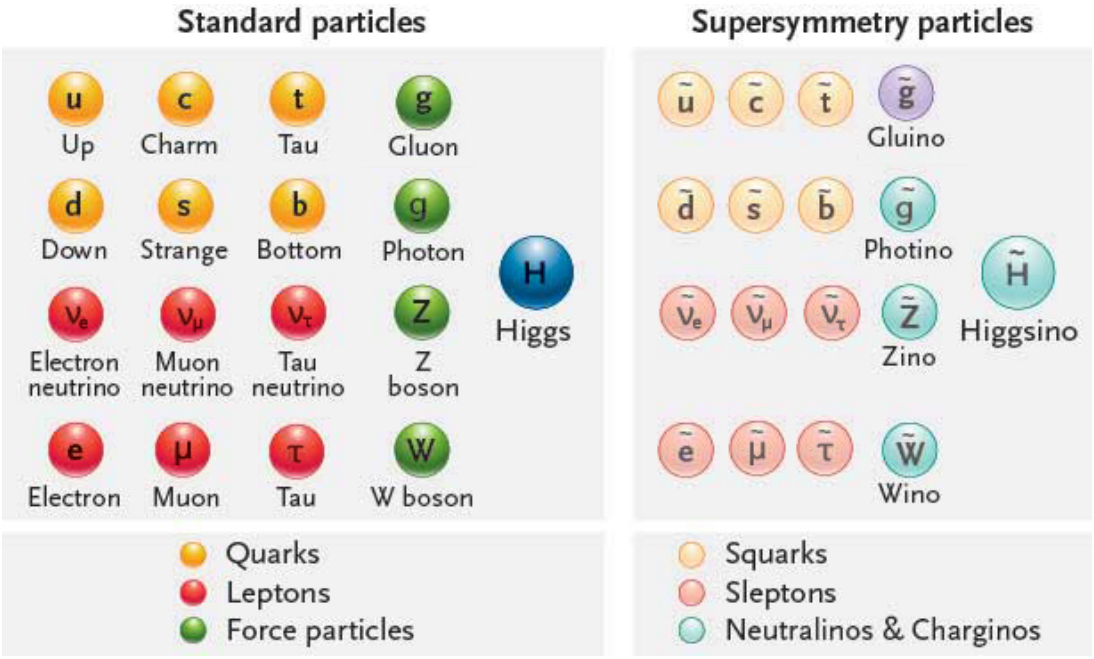

Figure 2: To every Standard Model particle a Supersymmetry particle with differing spin is assigned. [6].

The common notation convention is to put an "s" in front of the name to obtain a SUSY-boson name from a SM-fermion name (e.g. electron → selectron) or to add an "-ino" in the end of it to obtain a SUSY-fermion name from a SM-boson name (e.g. W → Wino). However, this is more of a rough rule of thumb than a strict law, since for example the superpartner of the photon is called photino and not photonino like one might assume because of the convention[2].

[2]The convention additionally is ambiguous for double-names like top-quark or tau-neutrino, because it is -in these cases- unclear where to put the "s" exactly. Surprisingly, the superpartner of the tau-neutrino is called a tau-sneutrino, but the one of the top-quark a stop-squark.

2.2 R-Parity and R-Parity-Violation

In case of the actual existence of supersymmetrical particles, the question arises, which types of processes with SUSY-particles in the initial and SM-particles in the final state can occur and vice versa. Especially the potential decay of supersymmetrical particles is to consider, since knowledge thereover would provide pieces of information about their stability, which is of interest in the context of dark matter. Introducing supersymmetrical particles also means introducing additional potential decay products for Standard Model particles. Since the stability of the proton (lifetime $\tau > 10^{31}$ years [7]) is an experimental fact, one has to provide a reason that it can however still not decay.
The question about the possibility of certain processes like the described ones can be traced back to the question about the conservation of a quantity, which is called R-parity and defined in a way, such that all SM-particles are of R-parity +1 and all SUSY-particles of R-parity −1:

$$R := (-1)^{3B+L+2S} \tag{1}$$

Hereby B denotes the baryon number, L the lepton number and S the spin. Because all of these quantities are additive quantum numbers, it follows that R is multiplicative [3]. This implies that, if R-Parity is conserved, SUSY-particles can only be created and destroyed in pairs. In this case the lightest supersymmetrical particle (LSP) is trivially stable, since it can neither decay into SM-particles due to the conservation of R-parity nor in SUSY-particles due to the conservation of energy.
Even though there is no experimental proof of a possible violation of the conservation of baryon and lepton number, there is also no symmetry associated with these artificially introduced quantum numbers like for energy, momentum and angular momentum. It is therefore not certain whether baryon and lepton number are indeed conserved.
This consideration motivates the construction of SUSY-theories, which take R-parity-violating [4] (RPV) scenarios into account as well. Signal samples of such a type produced with the aid of Monte Carlo simulation techniques are used in this analysis.

2.3 Accomplishments of and Experimental Evidence for SUSY

Supersymmetry is a popular[5] extension of the Standard Model, because its theoretical formulation brings some solutions to open questions with it.
First off, many SUSY-theories change the running of coupling constants as portrayed in figure 3 and accomplish the desired unification of electroweak and strong interaction.
Furthermore SUSY provides a solution to the hierarchy problem. Theories with R-parity-conservation can additionally explain the existence of dark matter with the LSP as

[3] Proof: consider the process X+Y → XY and define $A := 3B + L + 2S$ (only for reasons of convenience). Since B, L and S are additive, A is as well. Therefore:
$R_{XY} = (-1)^{A_{XY}} = (-1)^{A_X + A_Y} = (-1)^{A_X} \cdot (-1)^{A_Y} = R_X \cdot R_Y$

[4] This name may sound a little misleading, since actually R-parity-conservation and not R-parity is what is violated (or not).

[5] The 2014 edition of the Review of Particle Physics [1] by the Particle Data Group involves more than 120 papers dealing with SUSY.

WIMP-candidate. SUSY-versions with RPV-approaches do not necessarily do so, because in such scenarios the stability of the LSP is not granted.

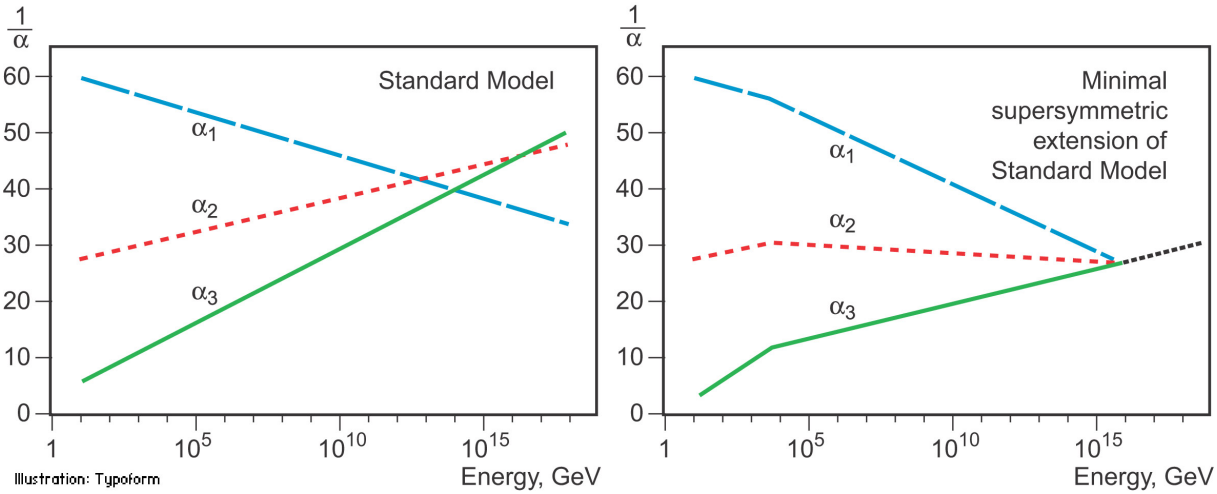

Figure 3: A comparison between the dependency of the different coupling constants α_i of the energy scale in the Standard Model and the MSSM as an example for a SUSY model (with a certain choice of parameters). Different colours (/indices) mark different forces: Blue - electromagnetic, red - weak, green - strong. The MSSM achieves a unification. [8].

In spite of all benefits, until now no supersymmetrical particles have been found in any experiment. This indisputable flaw might however merely be due to the fact that the masses of SUSY-particles could be higher than those which were already excluded experimentally (for exclusion limits see [9] for example). That the masses of the SM-particles and their superpartners apparently do not equal each other is unlike the difference in spin no byproduct of the construction of SUSY, but (in case of the validity of Supersymmetry) an experimental discovery, which means that the corresponding symmetry needs to be broken. Details of particular RPV-SUSY-theories like its mass hierarchy depend on the chosen breaking mechanism.

2.4 Details of the Discussed model

The particular RPV-SUSY-model considered in this analysis is adapted from [9]. The strengths of couplings between SM- and SUSY-particles are described by the coupling constants λ_{ijk} and λ'_{ijk} as parameters of the model with $i, j, k \in \{1, 2, 3\}$. The indices mark the generation and the prime indicates a production, whereas an unprimed lambda refers to a decay.
While all other supersymmetrical coupling constants remain 0, λ_{132}, λ_{231} and λ'_{311} are simultaneously set to a certain value (e.g. all are set to 0.01). Due to this choice of coupling constants (and correspondingly possible vertices) only lepton number and not also baryon number conservation is violated. This guarantees the experimentally verified stability of the proton.

The breaking mechanism is chosen in such a way that the SUSY mass hierarchy contains the tau-sneutrino as the LSP. Figure 4 gives an example of a process with a virtual particle of this kind. Note that the baryon number is conserved, whereas the conservation of lepton number is violated at both vertices.

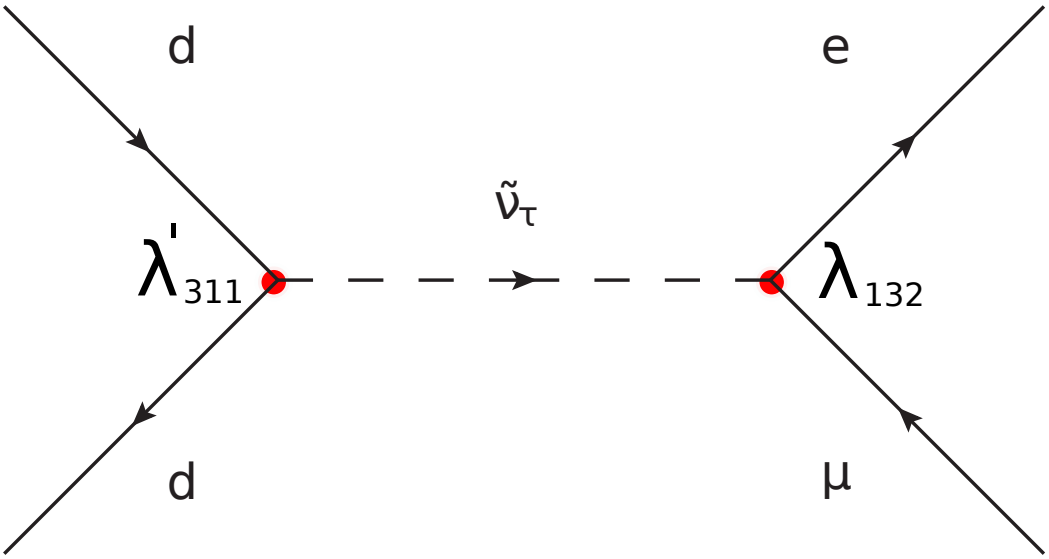

Figure 4: Feynman diagram showing the resonant production of a tau-sneutrino in the annihilation of a down quark with an anti down quark as well as its subsequent decay into an electron and antimuon. [9], modified.

As the model allows the tau-sneutrino to decay into an $e\bar{\mu}$-pair, one expects to observe a resonant signal production in the invariant mass distribution of the corresponding final state in Monte Carlo simulations of the model.

3 The Large Hadron Collider

One method of validating the Standard Model is conducting scattering experiments. Particles are accelerated to velocities close to the velocity of light and a collision at this speed is provoked. The thus achieved energies make the observation of rapidly decaying particles with rather high masses possible. The biggest facility dealing with these types of experiments in the world is the Large Hadron Collider (LHC) at CERN (Conseil Européen pour la Recherche Nucléaire) located near Geneva close to the border between Switzerland and France. As a proton-proton-accelerator with a circular geometry it requires two beam pipes under the influence of oppositely poled magnetic fields to keep the particles on their tracks. Currently a centre of mass energy of $\sqrt{s}$=13 TeV is achieved.
The LHC offers four spots for the observation of a crossing of beams called interaction points. At each of these points a detector is installed leading to four different autonomous experiments: A Large Ion Collider Experiment (ALICE) with the purpose to produce situations similar to those extremely shortly after the Big Bang [10], the Large Hadron Collider beauty (LHCb) specialized for processes involving bottom-quarks and aiming at a better understanding of the asymmetry between matter and antimatter in the universe [11] as well as ATLAS [12] and the Compact Muon Solenoid (CMS) [13], both constructed for collisions at extremely high energies [14]. An overview of the detectors and their positions relative to each other can be found in figure 5.

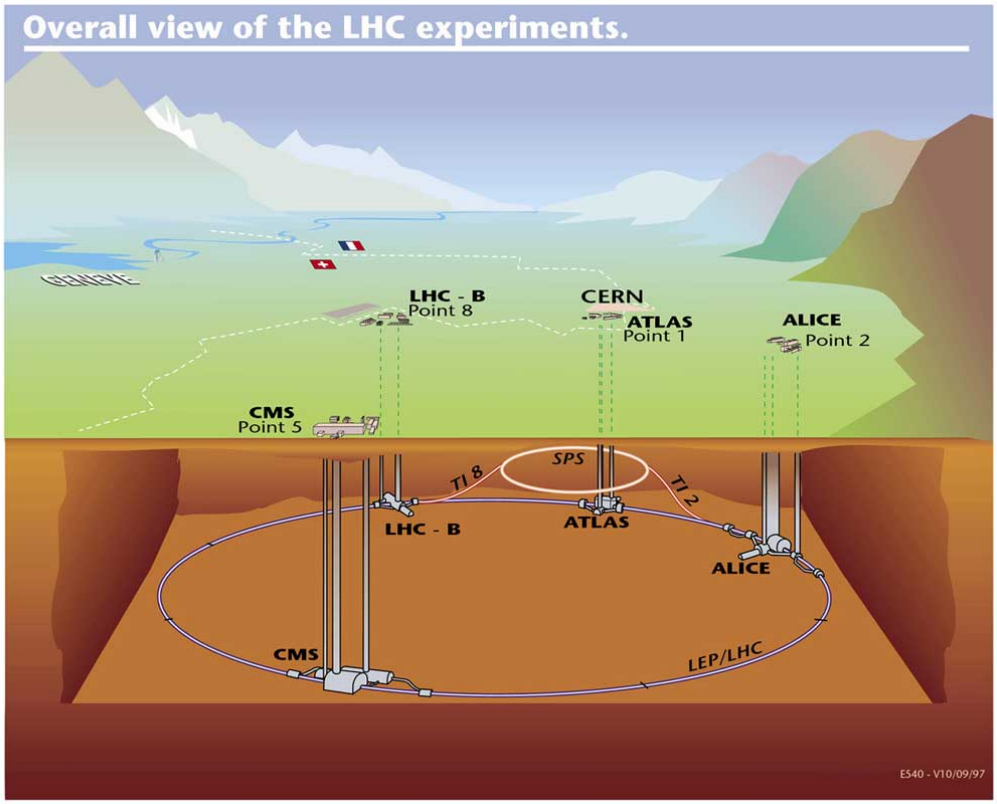

Figure 5: The LHC with its detectors ALICE, LHCb, ATLAS and CMS. [15].

4 The Compact Muon Solenoid

The Compact Muon Solenoid (CMS) is the detector of the LHC which produces the data analysed by the MUSiC-framework (this explains the "C" in MUSiC which is the acronym for "Model Unspecific Search in CMS"). It has a cylindrical form with a diameter of 14.6 m and a total length of 21.6 m [13]. Figure 6 shows a photo which gives an impression of these remarkable size dimensions.

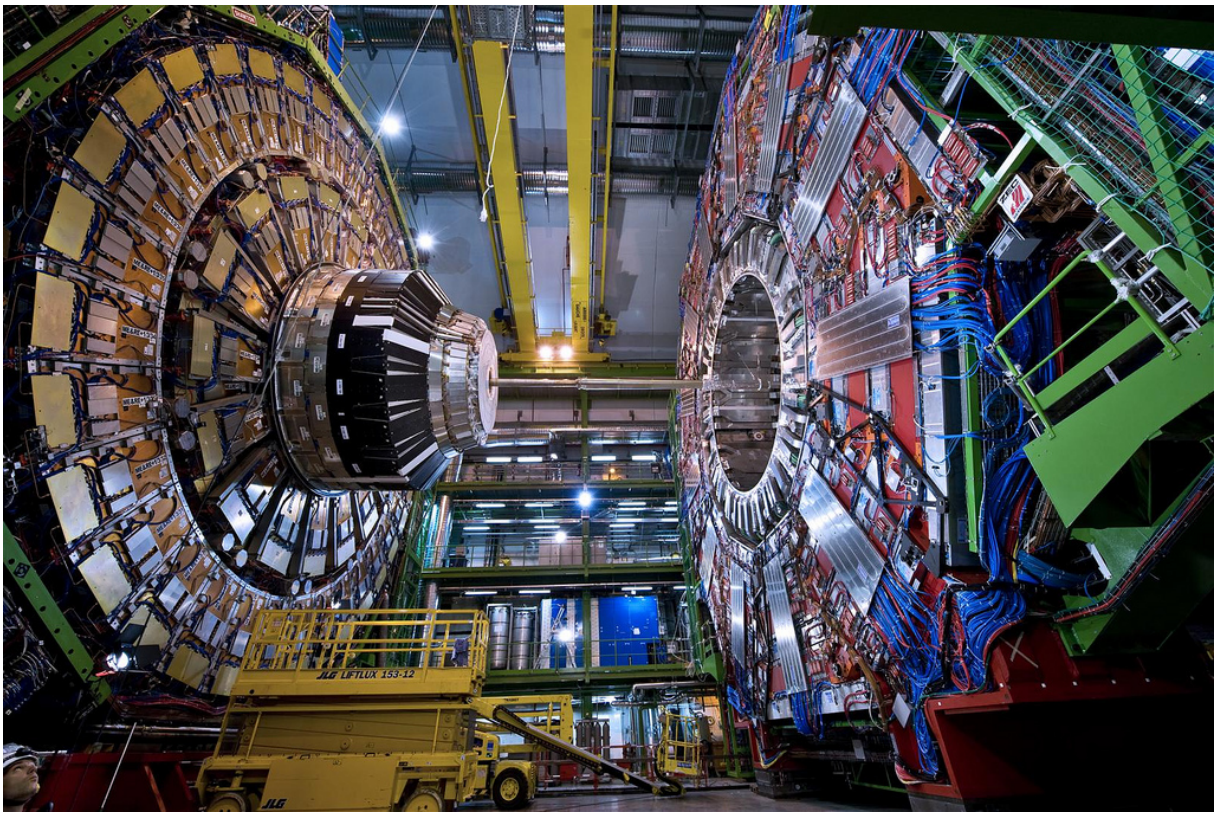

Figure 6: A picture of the CMS-detector before closure. The yellow vehicle and the human head in the lower left corner indicate the size of the solenoid. [17].

There are several detector components with different functions ordered around the beam centrically (the barrel) and at the ends of the cylinder (endcaps). Figure 7 shows the structure of the barrel and the way different types of particles behave in it. A superconducting solenoid generates a magnetic field to bend tracks of charged particles and thus enable a determination of the momentum and electric charge out of curvature radii. These radii are measured in the silicon tracker as the innermost component of the detector. Tracks are reconstructed by connecting single hits which are produced as electron-hole pairs in the active material.
To further characterise the particles both an electromagnetic and a hadron calorimeter (ECAL and HCAL) are installed between tracker and superconducting solenoid. Photons and electrons generate a shower of particles in the ECAL and hadrons in the HCAL. These showers cause the production of scintillation light which is then measured to obtain the energy deposit and thus the energy of the particles before traversing the detector. In combination with the depicted record of curvature radii a differentiation between photons and

electrons as well as charged and uncharged hadrons is possible. Both of the calorimeters are sufficiently large to cover so many radiation lengths that virtually all corresponding particles are stopped. The ECAL as the inner calorimeter additionally needs to have a long radiation length regarding hadrons so that hadrons are not already stopped there. It consists of lead tungstate crystals [13] which fulfil this requirement.

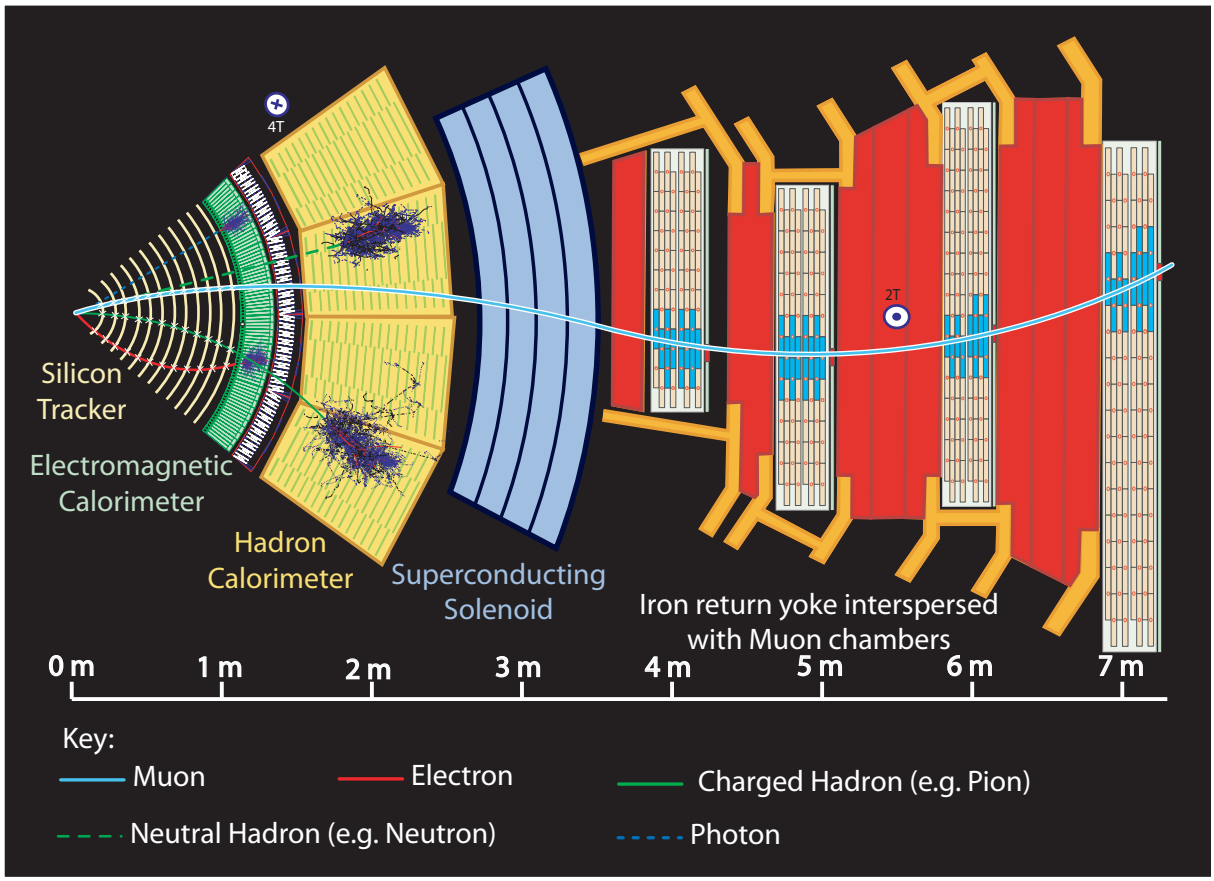

Figure 7: An overview of the diverse components of the barrel and the way different particles are detected. [18].

Muons and neutrinos however pass both calorimeters. While muons can bet tracked in the muon chambers which are embedded in the iron return yoke as the detector's outermost component, neutrinos stay completely undetected. Their appearance can only be concluded from the observation of missing transversal energy $\not{E}_T$.

5 Model Unspecific Search in CMS

The MUSiC-analysis has been developed in order to search for new physics (beyond the Standard Model of particle physics) in CMS data without an optimised search strategy for a specific BSM model. The latter circumstance is already included in the name, since the abbreviation “MUSiC“ stands for “Model Unspecific Search in CMS“ .
This chapter summarises the way the analysis works - in the following referred to as “the MUSiC-Workflow“ .
But first off a short motivation for a model unspecific search is provided.

5.1 Motivation

The usual approach to deal with CMS data pursued by dedicated analyses is to examine a certain proposal for new physics by taking a close look at the few final states in which the deviation is predicted to be the largest and to optimise the event selection to obtain a signal/background ratio which is as favorable as possible. However, this procedure comes with the disadvantage that plenty of experimental data is not taken into account at all, since only a fraction of all final states is considered. To focus on a specific theory of physics beyond the Standard Model directly from the start on additionally poses the risk to become blind for new physics scenarios not yet thought of.
The MUSiC approach on the other hand covers a wide range of final states which might lead to finding a global excess of deviations from the Standard Model expectation, even though the found deviations in single final states are not significant on their own. Even the experimental manifestations of theories not yet imagined might possibly be detected. These advantages are however accompanied by the disadvantage that conceivably only a smaller sensitivity can be achieved, because without a prediction the algorithm does not have any specific pattern to search for.

5.2 Initial Analysis Steps

In the beginning of the procedure, the measured data are firstly triggered to sort out very common processes and thus reduce the event rate. MUSiC uses single and double electron triggers as well as single and double muon triggers for this purpose.
Subsequently, the entirety of signals measured by the several components of the CMS-detector has to be associated with physical information, meaning the final states of all events in the accelerator have to be reconstructed. A rudimentary form of this object reconstruction has already been performed for triggering, but now a more sophisticated approach is pursued. As depicted in detail later, the analysis also requires pseudo-data generated by means of Monte Carlo Simulations according to the Standard Model to compare to the observed data. Only the availability of both pseudo- and observed data enables the algorithm to find potential deviations between the Standard Model and the experimental results at the LHC.

Before any data -be it recorded or simulated - can be analysed, its filesize has to be reduced so that it can be handled in a proper way with the available computer resources. This process is known as “skimming“ .
The occurrence of errors during the beforehand performed event reconstruction cannot be excluded which causes so-called fakes: particles being interpreted as different particles than they actually are. One can however apply object selection criteria to reduce these effects in a further step. This gain in purity has the disadvantage of a lower efficiency meaning less statistics, because events with relatively uncertain final states are sorted out completely. MUSiC chooses its object selection criteria in a way which attaches more importance to the purity than the efficiency. Selection requirements such as the track quality for muons and the shower shape for electrons and photons are used for the intended fake rejection. The investigated phase space is determined by the choice of “acceptance cuts“, which are listed in table 1.

Table 1: Acceptance Cuts

Object	$\frac{p_T}{GeV}$	η
e	> 25	$0 < \lvert\eta\rvert < 1.4442$; $1.566 < \lvert\eta\rvert < 2.5$
μ	> 25	$\lvert\eta\rvert < 2.4$
γ	> 25	$0 < \lvert\eta\rvert < 1.4442$
$jets$	> 50	$\lvert\eta\rvert < 2.4$
$\not\!\!E_T$	> 100	$\lvert\eta\rvert < 9999$

Note that missing transversal energy is regarded as a separate object in case it exceeds a threshold of 100 GeV. Furthermore MUSiC does not make a distinction between particles such as electron and positron (instead of e^- and e^+ there is only e). For the electron, values of $|\eta|$ around 1.5 are excluded. The purpose of this exclusion is to sort out objects which were detected close to the boundary between barrel and endcap.

5.3 Classification

To sort the reconstructed and skimmed events according to their final states, a so-called “classification“ is run: The events are assigned to both exclusive and inclusive event classes (exclusive: e.g. $1e + 1\mu$; inclusive: e.g. $1e + 1\mu + X$). Exclusive classes are only filled with events whose particles in the final state coincide exactly with the explicitly stated class components whereas the explicitly mentioned particles in the class definition of inclusive classes only need to be a subset of the particles in the final state to divide the corresponding event into the class.
Besides these two types of event classes, there is one further type: the jet-inclusive classes (e.g. $1e + 1\mu + Njets$). These are similar to simple inclusive classes with the difference

that the complement of the set of explicitly class defining particles and the set of particles in the final state of an event may only contain jets to assign the event to the class and not arbitrary objects.
An example for the procedure of classification is given in figure 8.

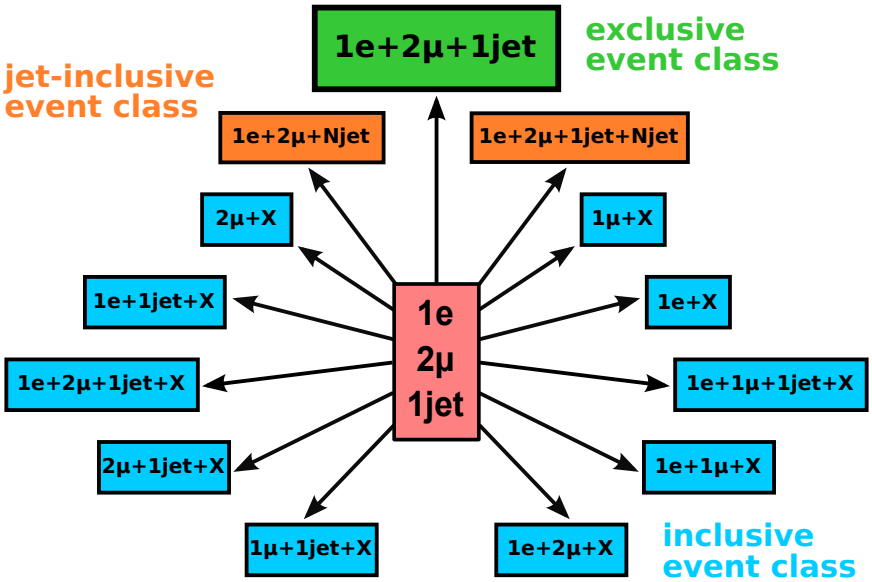

Figure 8: An example for a classification [23]: The event in question (red) has one electron, two muons and one jet in its final state. It is assigned to exactly one exclusive event class (green), two jet inclusive event classes (orange) and 10 (purely) inclusive event classes (blue). A generally valid relation between the number of exclusive classes N_{ex}, the number of jet inclusive classes N_{jet} and the number of (purely) inclusive classes N_{in}, one event is assigned to, is:
$1 = N_{ex} \leq N_{jet} \leq N_{in}$.

5.4 Kinematic Distributions and RoI-Scanner

In addition to the types of particles in the final state (e, μ, etc.), some of their reconstructed properties such as their momentum are at the disposal of the analyser. This information is used to calculate certain kinematic variables characteristic of the examined final state: the invariant mass M_{inv}, the sum of transversal momenta $\sum |p_T|$ and the missing transversal energy $\not{E}_T$. Note that the sums in the definitions of these variables only go over the explicitly mentioned particles in the class definition. In case that more objects of a type are present than stated in a (jet) inclusive event class name, these objects are ordered by p_T and the one(s) with the highest p_T are used for the summation.
Another subtlety is that for event classes with $\not{E}_T$-objects the invariant mass M_{inv} cannot be calculated. This problem originates from the fact that one does not know the momenta of the constituents of the colliding protons as incoming particles in the direction of the beam sufficiently exact, but only the parton distribution function (pdf) describing their statistical behaviour. However, in the case of no $\not{E}_T$-objects one can calculate M_{inv} out of the measured parameters in the final state. This is nonetheless not possible if there is a

$\not{E}_T$-object, for the corresponding momentum including its direction is unknown. Instead of the invariant mass M_{inv} the transversal mass M_T is therefore used as kinematic variable in such a case. Moreover, this case ($\not{E}_T$-object in the final state) is the only situation in which the distribution of $\not{E}_T$ is investigated, because for low values of missing transversal energy unwanted phenomenons like detector effects gain the upper hand.
In the further course of the analysis the deviation between real and simulated data is examined by taking a closer look at the distributions of the mentioned kinematic variables for a given class. Those distributions are binned according to the resolution with a minimum width of 10 GeV [6]. In such a histogram all possible connected regions of bins are investigated separately with one constraint: As for $\sum |p_T|$ and $\not{E}_T$ new physics are expected to show up in a rather broad deviation compared to $M_{inv/T}$, in these cases areas containing less than three bins are excluded.
The so-called "RoI-Scanner" ("RoI " for "Region of Interest") finds out in which region the deviation is least probable (see 9 for a visualisation). This probability is quantitatively expressed by a p-value which is defined in the following section - the smaller the p-value, the bigger the deviations and the more unlikely they are due to statistical fluctuations.

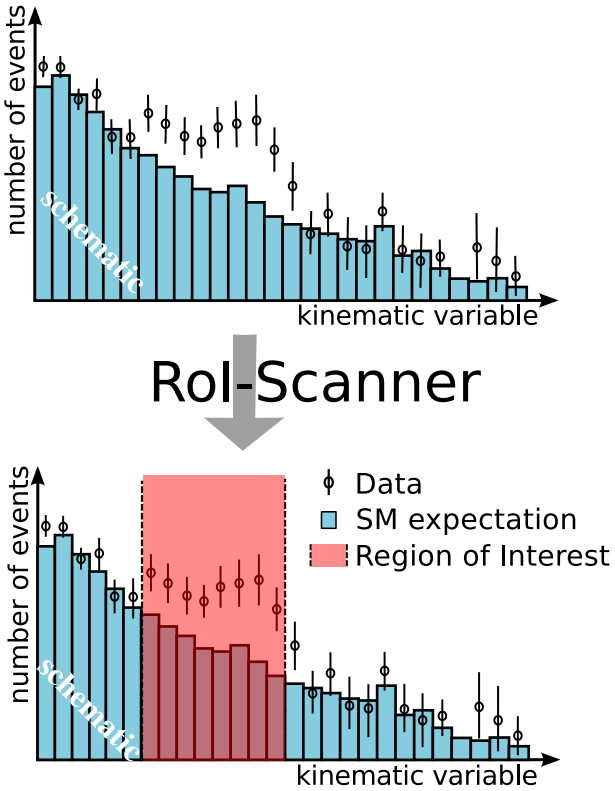

Figure 9: Exemplary kinematic distribution and functionality of the RoI-Scanner. For each class and each considered kinematic variable a distribution of the portrayed type is calculated. The RoI-Scanner finds the area with the largest deviation between data (points) and SM Monte Carlo (bins), the "Region of Interest"(RoI). [24], modified.

[6] For details see [14].

5.5 p-value

A p-value generally describes the probability to measure a certain value of an observable or a more extremely from a given theory expectation varying one under the assumption that this theory is correct. In the case investigated here the given theory is the Standard Model and the p-value is the probability to find the observed number of events N_{obs} or a higher (/lower) yield in a given region, given that the observed number is higher (/lower) than the (SM) expectation μ. Since considering the number of events means conducting a counting experiment, one might firstly assume a simple Poisson distribution:

$$p_{\text{preliminary}} = \begin{cases} \sum_{N=N_{\text{obs}}}^{\infty} \frac{e^{-\mu}\mu^N}{N!} & \text{if } N_{\text{obs}} \geq \mu \\ \sum_{N=0}^{N_{\text{obs}}} \frac{e^{-\mu}\mu^N}{N!} & \text{if } N_{\text{obs}} < \mu \end{cases} \tag{2}$$

However, there is no exact expectation value μ, because μ is obtained from SM Monte Carlo simulations which vary within their systematic uncertainties. The distribution function for μ can be approximated as a Gaussian function, which however has to be truncated at zero to account for the fact, that μ is non-negative. Its mean value is denoted by N_{SM} and the systematical uncertainty by σ_{SM} (for details on systematics see 5.8). To obtain a final result for p, the Gaussian function is convoluted with the Poisson distribution (the factor C has to be introduced to ensure normalisation):

$$p = \begin{cases} \sum_{N=N_{\text{obs}}}^{\infty} C \cdot \int_0^{\infty} d\mu \, \exp\left(-\frac{(\mu - N_{\text{SM}})^2}{2\sigma_{\text{SM}}^2}\right) \cdot \frac{e^{-\mu}\mu^N}{N!} & \text{if } N_{\text{obs}} \geq N_{\text{SM}} \\ \sum_{N=0}^{N_{\text{obs}}} C \cdot \int_0^{\infty} d\mu \, \exp\left(-\frac{(\mu - N_{\text{SM}})^2}{2\sigma_{\text{SM}}^2}\right) \cdot \frac{e^{-\mu}\mu^N}{N!} & \text{if } N_{\text{obs}} < N_{\text{SM}} \end{cases} \tag{3}$$

For every region a p-value is calculated, but only the smallest one (determined by the RoI-Scanner) is used in the further course of the analysis, to avoid correlation, since the regions partly overlap.

5.6 $\tilde{p}$-value

With increasing number of contemplable areas it becomes more and more probable, that the scanner finds one with a low p-value (this phenomenon is known as "Look-elsewhere-effect"). To nevertheless obtain a meaningful result for the degree of deviation from the expectation, one has to take this effect into account. This is done by converting the p-value into a $\tilde{p}$-value, which is basically nothing else than a corrected version of the p-value.
For this purpose so-called pseudo-experiments are conducted: MUSiC dices the SM Monte Carlo sample (for details on dicing see section 5.8). The resulting distribution is then used in the above described way as if it was the data input. This procedure enables MUSiC to get an impression of how small p-values get merely due to statistical fluctuations, since basically the same samples are compared. A preferably big number of pseudo-experiments

is conducted- each yielding one final p-value which is then called p_{pseudo}.
The information generated in this way is subsequently used to correct the original p-value (for reasons of differentiation now called p_{data}) to the $\tilde{p}$-value:

$$\tilde{p} = \frac{\#p_{pseudo} : p_{pseudo} \leq p_{data}}{\#p_{pseudo}} \tag{4}$$

Note that $\tilde{p}$ can be interpreted as a p-value in the above defined sense, because if the Standard Model is correct, data- und pseudo-experiment-sample resemble each other so that an average p-data-value is the expectation for the p-pseudo-value. In case of sufficiently high $\#p_{pseudo}$, the right hand side of the stated formula predicts the probability that a single p-pseudo-value is equally small or smaller than p-data. But this is just the "probability to measure a certain value of an observable or a more extremely [...] varying one" from the p-value definition, because a smaller p-value always means a more extreme deviation. However, the formula is not correct in case no p_{pseudo} is smaller than p_{data} (or equally small), because the quantity which should be described by the formula has characteristics of a p-value and can therefore never reach zero, since the probability to measure something at least as or more extreme does actually never vanish, but at most become arbitrarily small. This circumstance is included in the MUSiC analysis in the following way: in case the formula gives 0, $\tilde{p}$ is artificially set to $\frac{1}{\#p_{pseudo}}$. This value is more of an upper boundary for the actual $\tilde{p}$, which is preferred over a lower boundary, which 0 would be, because the deviations are thus made smaller instead of bigger. The error of seeing no deviation, even though there is one, is thus chosen as more favorable than the error of seeing a deviation, even though there is none.
A schematic illustration of the construction of $\tilde{p}$ is shown in figure 10. The x-axis shows the negative decadic logarithm of p_{pseudo} which stays positive because of $p \leq 1$. Since $-log$ is strictly monotonically decreasing, p_{pseudo} decreases from the left to the right. The logarithmic scale is chosen in order to provide more horizontal space to the lowest p-values, because these are the ones caused by the strongest deviations and therefore of the highest interest. The y-axis is scaled logarithmically as well, in this case to make a clearly visible illustration of the event numbers of all different p_{pseudo}-regimes possible, even though they differ by several orders of magnitude.
With the described method one finally obtains one $\tilde{p}$-value for each class.

5.7 $\tilde{p}$-distribution

Similar to avoiding the bias of particularly choosing the region with the lowest p-value without accounting for the effect that in many regions the occurrence of some small p-values is expected which motivated the step $p \to \tilde{p}$, another statistical caveat needs to be considered: Because there are typically very many classes ($\mathcal{O}(100)$), it is expected to observe some classes with rather low $\tilde{p}$-values. It is therefore necessary to take a multitude of classes into consideration, which is however what was planned anyway in order to be sensitive to small deviations in many final states.
One possibility is to only make use of all exclusive classes. This is however problematic, because some processes have known issues with the description of jet multiplicity, since higher order QCD effects gain importance for increasing jet number. All exclusive classes

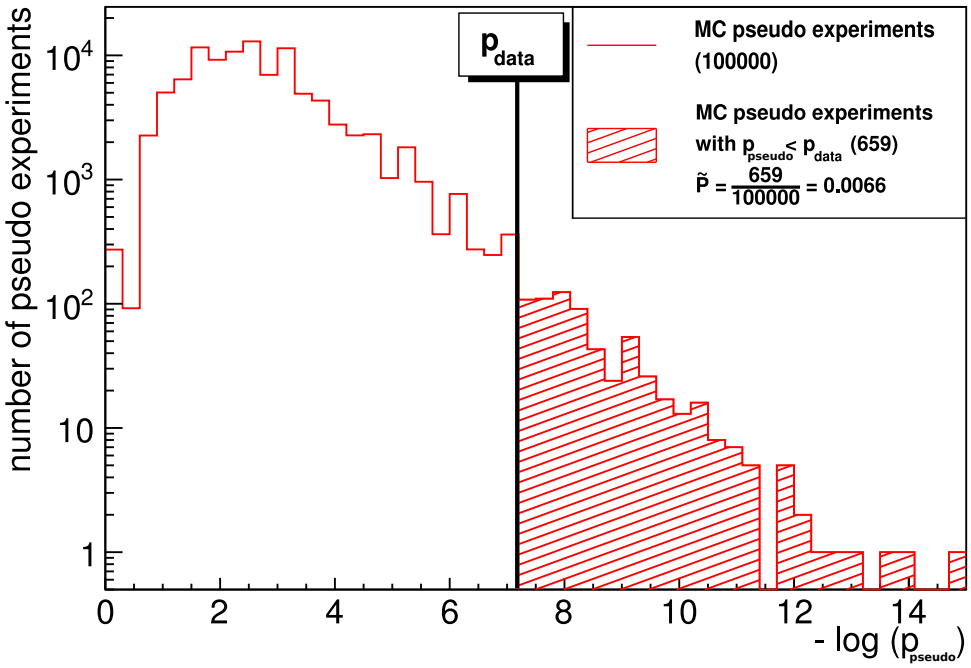

Figure 10: Graphical interpretation of the construction of $\tilde{p}$: $\tilde{p}$ can be calculated as the number of events in the shaded regime divided by the total number of events (=number of events in the whole regime). [22], modified.

with more than five jets are therefore replaced by the one inclusive class $6jets + X$. The set of classes obtained on this way is referred to as the "exclusive variant" in the further course of this thesis.
The $\tilde{p}$-values of the stated classes are now plotted in a single histogram (data vs. MC). To enable a comparison the whole workflow is also run with a SM Monte Carlo sample as data input yielding a second histogram (MC vs. MC). There is however an arbitrary number of SM Monte Carlo distributions at the disposal of the analyser (these distributions already had to be diced to obtain the p_{pseudo}-values). MUSiC therefore creates a multitude of MC vs. MC histograms. All of these are combined to a single one with bars by applying the following method: In a given bin the algorithm firstly computes the median of all bin heights coming from the different dicing rounds. In order to build intervals with a meaning similar to the one of a one sigma environment, both above and below the median 34% of the outcomes for different dicing rounds are determined, yielding 68% in total. Bars are drawn between the thus found highest and lowest numbers of classes per dicing round. This procedure is repeated for every bin and also conducted with an interval of 95%. Due to the stated construction rule the bars do not necessarily have to be symmetric, because the event numbers for different signal dicing rounds might be concentrated more densely above the median than below (or vice versa). The mean value is additionally indicated, but the bars refer to the median. MC vs. MC therefore includes two graphs: mean pseudo rounds and median pseudo rounds. Both of them are plotted in one figure as well as the stated environments and the data vs. MC histogram. An example of such a $\tilde{p}$-distribution can be found in 11 . The scaling of the axes is chosen like in figure 10 for the same reasons.

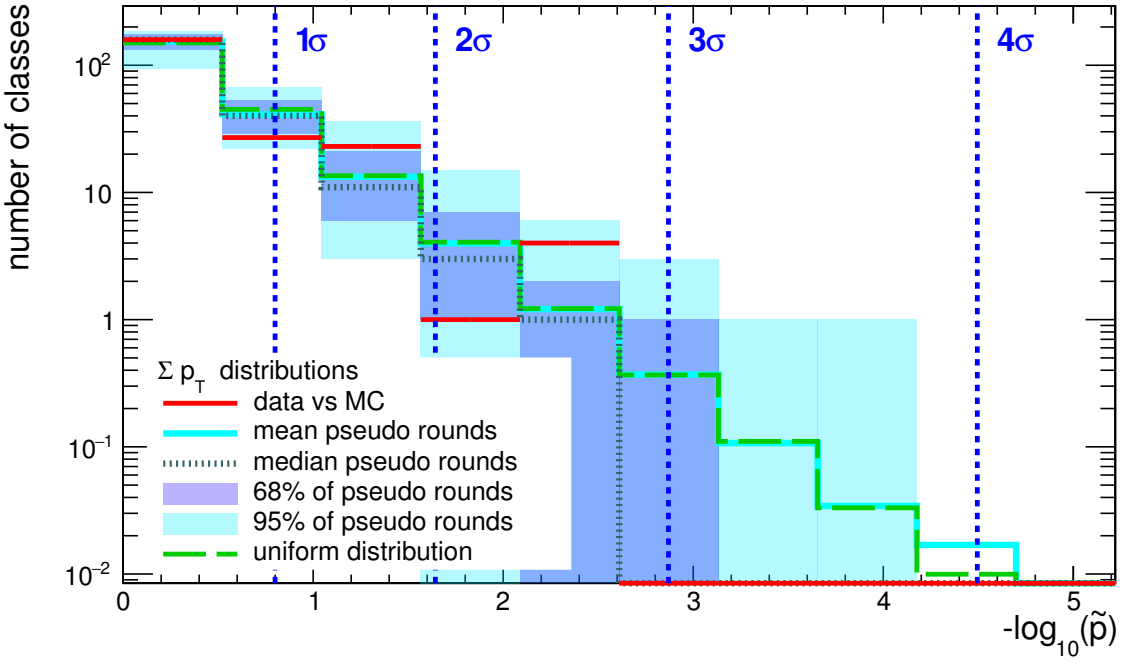

Figure 11: An example for a $\tilde{p}$-distribution. Such a plot is produced for each considered kinematic variable. This one contains schematic results for $\sum p_T$.

Under the assumption that the null hypothesis is correct, p-values follow a uniform distribution between 0 and 1. One therefore expects that the MC vs. MC histogram resembles such a distribution, since using MC as input of a comparison with MC corresponds to having a correct null hypothesis. To verify this expectation, a uniform distribution is additionally plotted into the figure. Because of the scaling of axes the bins of the uniform distribution are of different sizes: The number of classes against $\tilde{p}$ itself would give a histogram with same sized bins, but the logarithmic scaling of the x-axis causes that $\tilde{p}$-regimes with different widths are taken together to $-log(\tilde{p})$-regimes of same widths. The total number of classes therefore becomes dependent on the considered bin. This yields the shown graph with the shape of stairs.
As a further feature the $\tilde{p}$-distribution includes several vertical dotted lines with the following meaning: It is expected that 68% of all classes yield a $\tilde{p}$-value which is smaller than the one marked by the 1σ line. Correspondingly, about 95.5% should give a $\tilde{p}$ which is smaller than the one marked by the 2σ line and so on.
Besides the stated exclusive version as choice of the considered event classes, a further possibility is to make use of inclusive event classes. This leads to correlation effects, because most events are assigned to more than one inclusive class (see 8), so that the events in differing inclusive classes partly overlap. However, this does not really cause a problem, since the correlation enters the analysis in both data vs. MC and MC vs. MC, which is why it is automatically accounted for in the final outcome. This choice of considered event classes is called “inclusive variant“ in the further course of this thesis. The issue with final states containing many jets is treated in a similar way like in the exclusive variant.

5.8 Systematics and Dicing

The number of events in a bin as a physical variable has various systematic error sources which can be divided into experimental and theoretical ones. The error on the luminosity is an example for the former kind, the error on the cross section is of the latter type. In a pseudo-experiment all quantities q_i with influence on the number of events in a bin are shifted within their (experimental or theoretical) uncertainties. This process is called "dicing", because the shift parameter is determined by coincidence. MUSiC uses a normal distribution ($\mu = 0$; $\sigma = 1$) as its probability density function. In every pseudo-experiment (or equivalently dicing-round) one shift factor α_i is diced for every q_i and then applied to all bins. The bins are thus assumed to be fully correlated. The systematic uncertainty σ_{q_i} on each q_i leads to a systematic uncertainty n_i on the number of events. Unlike the shift factor α_i both of these quantities can differ in different bins. The values of α_i and n_i are multiplied to obtain the additive correction on the mean of event numbers in a bin stemming from the quantity q_i. Taking all error sources into consideration and marking the dependency of bins with the additional index j, this consideration yields the following formula for the relation of the number of events before ($N_{j,\text{old}}$) and after ($N_{j,\text{new}}$) the dicing-round in the bin indexed with j:

$$N_{j,\text{new}} = N_{j,\text{old}} + \sum_{i=1}^{\#q_i} \alpha_i \cdot n_{i,j} \tag{5}$$

The obtained result represents a situation in which a certain systematic shift has been performed and is now fixed. The final number of events in a bin can however still vary due to statistics. To incorporate statistical effects, each $N_{j,\text{new}}$ is regarded as mean value of a Poisson distribution. A statistical dicing is performed according to this distribution function. Unlike the systematical dicing, for which the diced parameters α_i were independent of the bin-index j, the statistical dicing is performed individually in each bin.
Dicing distributions from Monte Carlo samples is a common method in the MUSiC analysis. It is used both in the already depicted workflow and in the features added for sensitivity studies which are described in the next section.

6 Signal Studies

6.1 Motivation

Assuming that a certain BSM model is actually realised in nature and therefore also valid in the range of the CMS experiment, it is still first off unclear, if -and if yes, in how far- the discrepancy between this model and the Standard Model becomes visible in the $\tilde{p}$-distribution as the final outcome of the MUSiC analysis.
The aim of this thesis is to investigate this question by conducting a sensitivity study: Instead of actually observed data, known signals (merged with the SM background) are used as data input. This procedure makes it possible to gain knowledge about what properties a signal must have in order to be clearly visible in the $\tilde{p}$-distribution.

6.2 Adaptations of the $\tilde{p}$-distribution for Signal Studies

Using an artificially produced signal (merged with the SM background) as data input instead of actually observed data introduces some new possibilities in the context of the $\tilde{p}$-distribution. Since the signal is the product of a Monte Carlo simulation, it can be diced like the SM samples used in the MUSiC-workflow. This makes it possible to obtain an arbitrary number of $\tilde{p}$-distributions out of one signal sample. One can therefore include bars for the signal by combining these distributions to a single one with the same method used for MC vs. MC and described in 5.7. There is however the difference that only an environment containing 68% of dicing rounds is drawn and not also an environment with 95%. Additionally, the environment is plotted differently (more in the style of an errorbar, even if the environments are no errorbars in a real sense) and the cases "mean signal rounds" and "median signal rounds" are separated into two different $\tilde{p}$-plots. In each of these the bars are then constructed based on the result for the corresponding quantity (mean or median). Note that an interval construction for the mean analogously to the one depicted above for the median is not always possible, since it is not granted that the mean lies at a point in the set of class numbers so that both above and below it at least 34% of the values for different dicing rounds are positioned. However, in the cases considered here no problems occur.

6.3 Used Signal Samples

As announced in the introductory section about Supersymmetry, the used signal samples are based on the RPV model adapted from [9]. One might possibly wonder about if this does not contradict the concept of MUSiC as a model unspecific approach, because the sensitivity is now only tested for a particular model.
Even though the signal sample as data input is based on a new physics theory, the workflow

itself is still run completely independent of a BSM model. In addition, some of the results might also allow conclusions on the sensitivity of MUSiC for models which in principle differ a lot from the RPV model, but show similar signals in the kinematic distributions for certain final states. Even if the final state with a similar deviation is a different one, the sensitivity should be comparable, because all considered classes are taken into account equally in the $\tilde{p}$-plot by yielding exactly one $\tilde{p}$-value.
The exact names of the used samples can be found in the appendix. In all considered cases (M_{inv} /$\sum p_T$, median /mean, exclusive variant /inclusive variant) 200 signal and 50000 pseudo dicing rounds are conducted. The parameters of the RPV model are treated in the following way: for coupling constants fixed at $\lambda_{132} = \lambda_{231} = \lambda'_{311} = 0.01$ the mass of the tau-sneutrino ($M_{\tilde{\nu}_\tau}$) is varied: Mass points of 500 GeV, 700 GeV and 1000 GeV are investigated, each yielding a separate histogram.

6.4 Final Plot and Qualitative Discussion of the Sensitivity

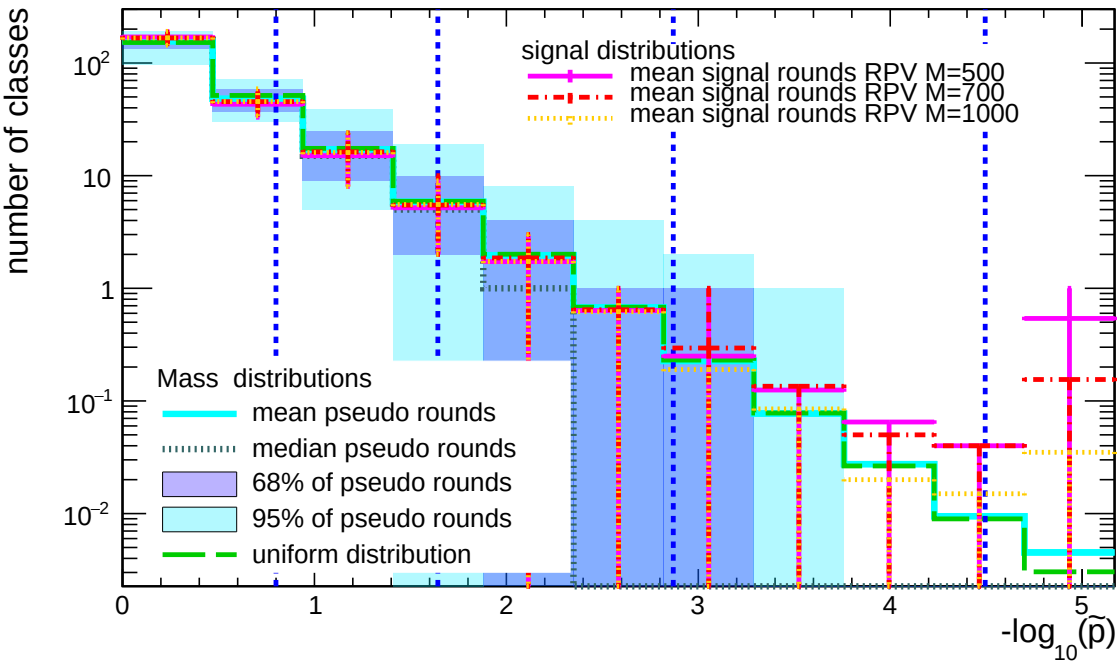

Figure 12: The final outcome for the adapted $\tilde{p}$-distribution with the mean value as considered statistical quantity, M_{inv} as kinematic variable and the exclusive variant as choice of event classes.

Figure 12 shows the final outcome for the $\tilde{p}$-plot with the exclusive variant, M_{inv} as kinematic variable and the mean value used for the combining of different signal rounds. For all considered tau-sneutrinos masses a clear deviation between Standard Model and RPV theory becomes visible. The corresponding RPV bins on the right side are higher which means that there are more classes with small $\tilde{p}$-values and therefore larger deviations in the kinematic distributions than for MC vs. MC. However, the difference of the signal and pseudo rounds histograms only seem so extreme because of the scaling of the y-axis.

In all three cases the last bin actually only differs by less than one class and the bins on the right side taken together still contain few classes with noticeably smaller $\tilde{p}$. This behaviour nonetheless corresponds exactly to the expectation, because one suspects to find large deviations merely in few final states, since only few couplings between SM and SUSY particles are set to values unlike zero. This way also a little number of vertices and therefore beforehand impossible processes becomes possible. As indicated in section 2.4 such a process is for example the resonant signal production expected in the exclusive class $e + \mu$ (remember that MUSiC makes no difference between μ and $\bar{\mu}$). Many final states nevertheless remain more or less untouched by the introduction of the few supersymmetrical couplings.
Even though the introduction of supersymmetrical couplings thus only effects few classes, the deviation becomes clearly visible in the $\tilde{p}$-distribution for sufficiently low masses $M_{\tilde{\nu}_\tau}$. For MUSiC is able to find the deviations in the few final states, it is clearly sensitive for the total deviation caused by such a type of BSM model with such a choice of parameters. For increasing $M_{\tilde{\nu}_\tau}$ the deviations in the kinematic variables of the affected classes decrease and MUSiC becomes more and more insensitive: the histograms signal vs. MC and MC vs. MC near each other.
The exclusion limit for the tau-sneutrino mass achieved by the authors of paper [9] is 1000 GeV. According to this, MUSiC achieves an equally high sensitivity regarding the considered RPV model, because even 1000 GeV as the highest mass considered shows a visible deviation in the $\tilde{p}$-plot, even if it is small compared to the ones obtained for lower masses. Note however that the workflow of dedicated analyses is specialised on a particular BSM theory, which is why MUSiC cannot achieve comparable sensitivities in general. An advantage of MUSiC on the other hand becomes clear when considering the following scenario: data observed at CMS corresponds to a certain new physics model, but this model has not been proposed by theorists yet. Since the signals caused by it are different from those caused by the models investigated by dedicated analyses, these analyses are not able to find a significant deviation from the Standard Model. In case the experimental ramifications of the BSM scenario are however sufficiently large, the $\tilde{p}$-distribution of MUSiC might possibly show a visible deviation in total. A problem could be that it however would then first off be completely unclear, where this deviation comes from and how the theory causing it might look like. But one could at least find out the classes with the lowest $\tilde{p}$ and thus gain some hints what to look for exactly. This "writing back" of event classes is discussed in section 6.7.

6.5 Mean or median

Figure 13 shows the final outcome for the $\tilde{p}$-plot with M_{inv} as kinematic variable and the median used for the combining of different signal rounds. The plots with both mean and median are considered because it was first off unclear which of these quantities is better applicable for the purpose of the analysis.
A major difference between median and mean value is that the outliers of a sample do not influence the median at all, since building the median means picking out the most central value (or the mean of the two most central values in case of an even sample size). This property has both disadvantages and advantages: On the one hand, plenty of information is

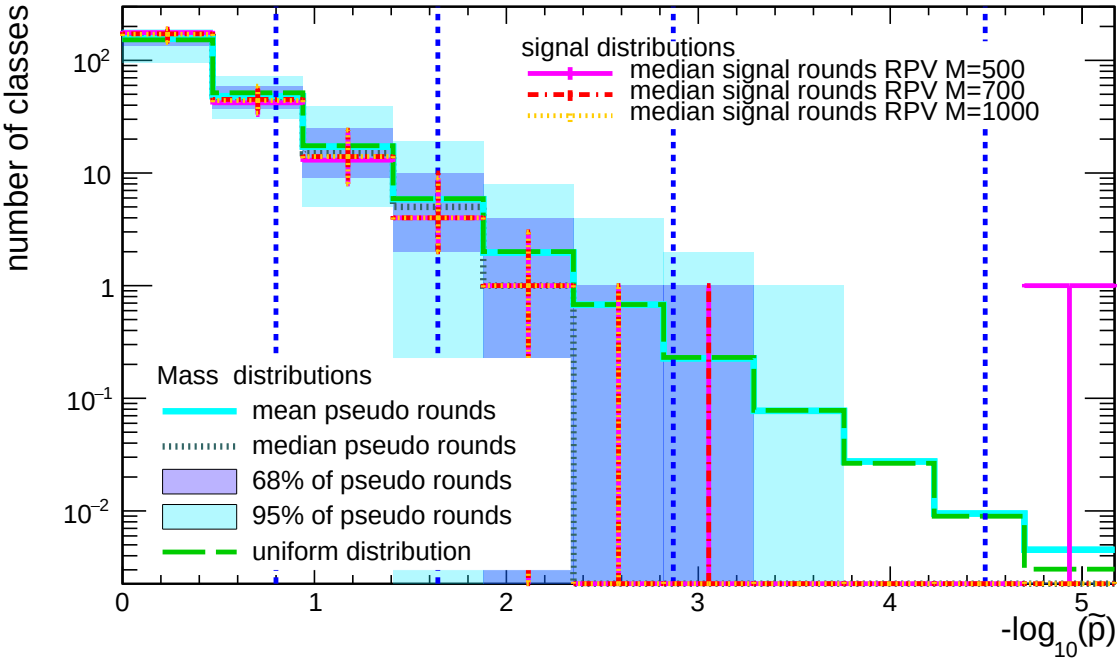

Figure 13: The final outcome for the adapted $\tilde{p}$-distribution with the median as considered statistical quantity, M_{inv} as kinematic variable and the exclusive variant as choice of event classes.

lost, because the majority of values in the sample only enters the calculation by influencing the order of values and thus which particular value is finally picked. It does not make any difference for the median, if the biggest value is 100 or 1000000000[7].
On the other hand, it is sometimes preferable not to take the outliers into consideration. Especially in case of extremely unsymmetrical distributions with outliers the mean value loses much of its expressiveness. For example in case of a sample size of 100 with 99 times 0 as result and one time 10000 the mean value is 100 and therefore not really close to any of the 100 given values.
A further difference is the following: because all single results are numbers of classes and therefore natural numbers (or zero), the median can only be a natural number (or zero) as well (or additionally a natural number minus 0.5 in case of an even sample size). In every case the possible values of the median are highly discrete, whereas the mean value can take arbitrary positive real numbers (including zero). Especially in the case of very small values in the sample (e.g. most of them being 0 and 1) the median can suddenly change extremely compared to the values of the sample by just a little change of the set of values (e.g. $0, 0, 0, 1, 1 \Rightarrow \text{median} = 0$; $0, 0, 1, 1, 1 \Rightarrow \text{median} = 1$). Such a sudden change however becomes increasingly improbable for bigger sample sizes.
The mean on the other hand is not that sensitive to such little changes of the set of values (in the example the mean value changes from 0.4 to 0.6). Since a case like the stated one (only small numbers in the sample) can occur in the MUSiC analysis, namely in the rightmost bin of the $\tilde{p}$-plot for example, this effect is to consider. A disadvantage of the

[7] At least in case of a sample size bigger than two, which can (and is) always achieved by the choice of both signal and pseudo dicing rounds.

mean is however that (in the very probable case it is not an integer) it could never be the result of a single dicing round, but is more of an artificially constructed value. In case of an odd number of sample sizes, it is granted that the median could also be the outcome of a single dicing round (and in the considered case it is also very probable for even numbers of sample sizes).

6.6 Quantitative Discussion of the Sensitivity

In order to obtain some kind of measure for the extent of deviation for the different mass points, a χ^2 test is performed. As input variables the median (or mean respectively) of the number of classes for signal rounds S_i and for pseudo rounds P_i in the bin indexed with i are used (for pseudo rounds always the median is chosen). Since one has to account for the fact that the σ environments are not symmetric like depicted above, the half length I_i of the constructed whole interval is plugged in the denominator, whereby the intervals for the pseudo rounds are chosen:

$$\chi^2 = \sum_{i=1}^{N} \frac{(S_i - P_i)^2}{I_i^2} \tag{6}$$

The upper summation limit N is the number of bins ("bins" with a height of zero are not regarded as such). To avoid a strong dependency of the binning, χ^2 is additionally divided by N. Calculation yields the results presented in the tables 2 and 3.

Table 2: $\frac{\chi^2}{N}$ for the mean with M_{inv} as kinematic variable and the exclusive variant

$M_{\tilde{\nu}_\tau}$	500 GeV	700 GeV	1000 GeV
$\frac{\chi^2}{N}$	0.329	0.332	0.278

Table 3: $\frac{\chi^2}{N}$ for the median with M_{inv} as kinematic variable and the exclusive variant

$M_{\tilde{\nu}_\tau}$	500 GeV	700 GeV	1000 GeV
$\frac{\chi^2}{N}$	0.118	0.052	0.048

The results roughly correspond to the expectation and observation in the $\tilde{p}$-plot that the deviation between signal vs. MC and MC vs. MC decreases for increasing masses. For values of $\frac{\chi^2}{N}$ in different cases (e.g. Sum of transversal momenta in the inclusive variant) consult the appendix.

6.7 Writing Back of the Most Significant Event Classes

Determining the classes with the lowest $\tilde{p}$-values yields the final states with the highest deviations. Both the class $e + \mu$ in the exclusive variant and the class $e + \mu + X$ in the inclusive variant belong to the most significant ones. This corresponds to the assumption uttered in section 2.4 because of the fact that a tau-sneutrino can decay into such a final state. Due to this decay mode it is expected to observe the tau-sneutrino in the invariant mass spectrum of the stated final state as a resonance. In order to demonstrate the thus caused deviation between RPV theory and Standard Model the invariant mass distribution is plotted for the exclusive class $e + \mu$ for each of the three different masses in the figures 14, 15 and 16. The RPV signals (dark grey) are clearly positioned at the respective values of the tau-sneutrino mass.

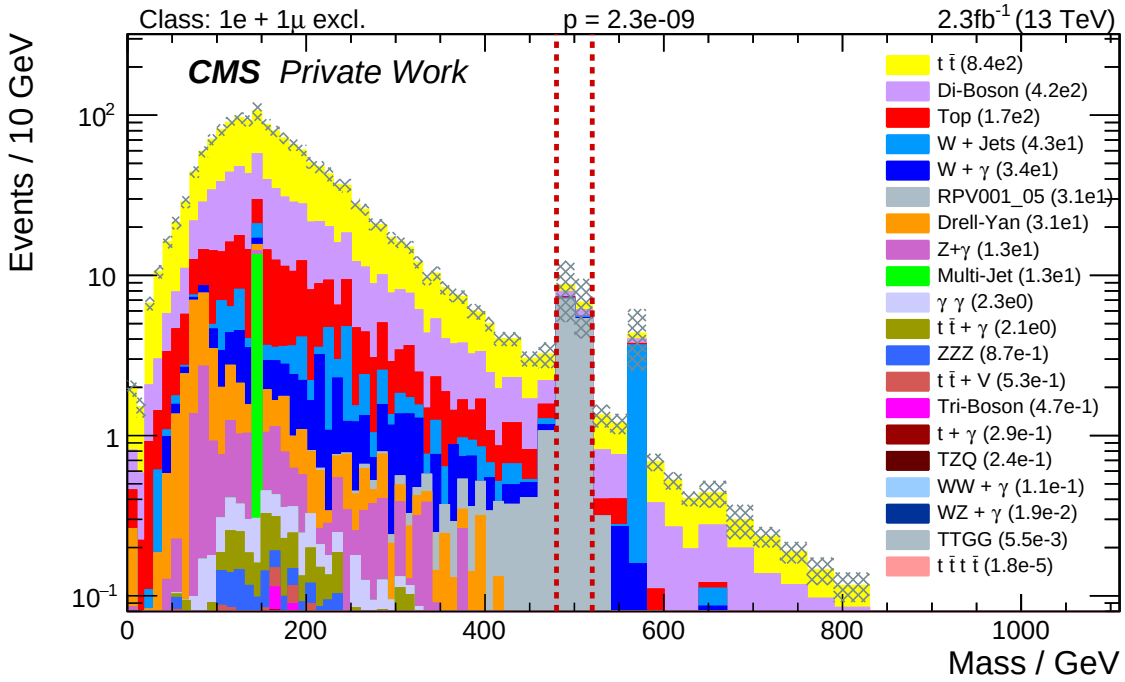

Figure 14: Invariant mass distribution of the exclusive event class $e + \mu$, $M_{\tilde{\nu}_\tau} = 500\,\text{GeV}$

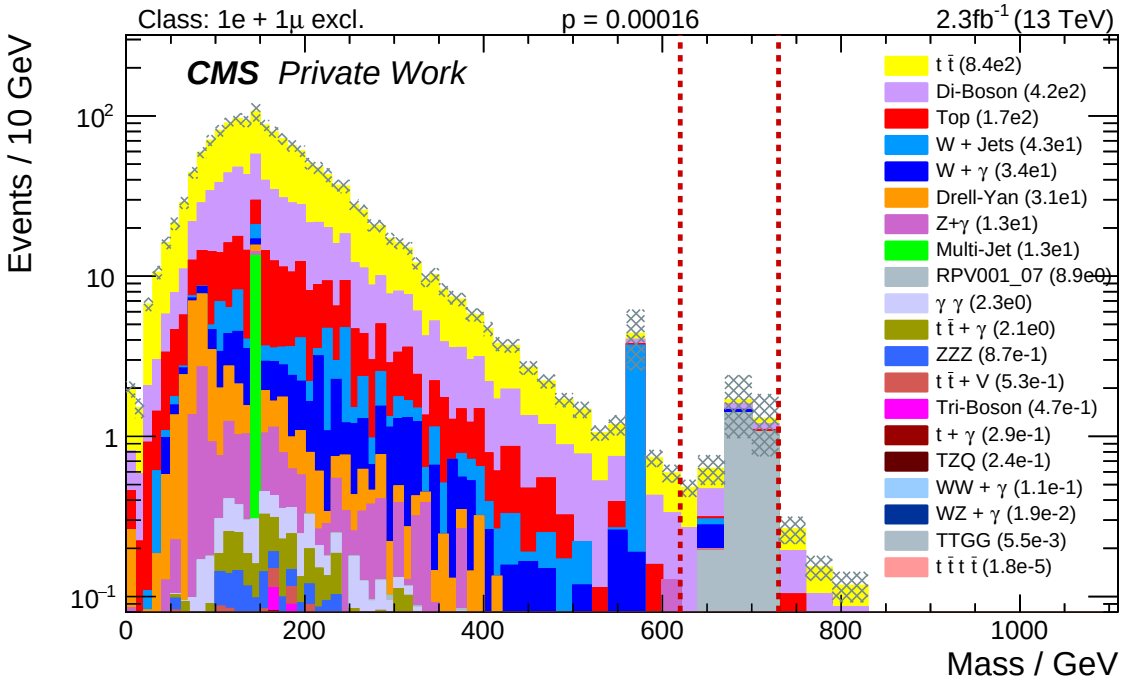

Figure 15: Invariant mass distribution of the exclusive event class $e + \mu$, $M_{\bar{\nu}_\tau} = 700\,\text{GeV}$

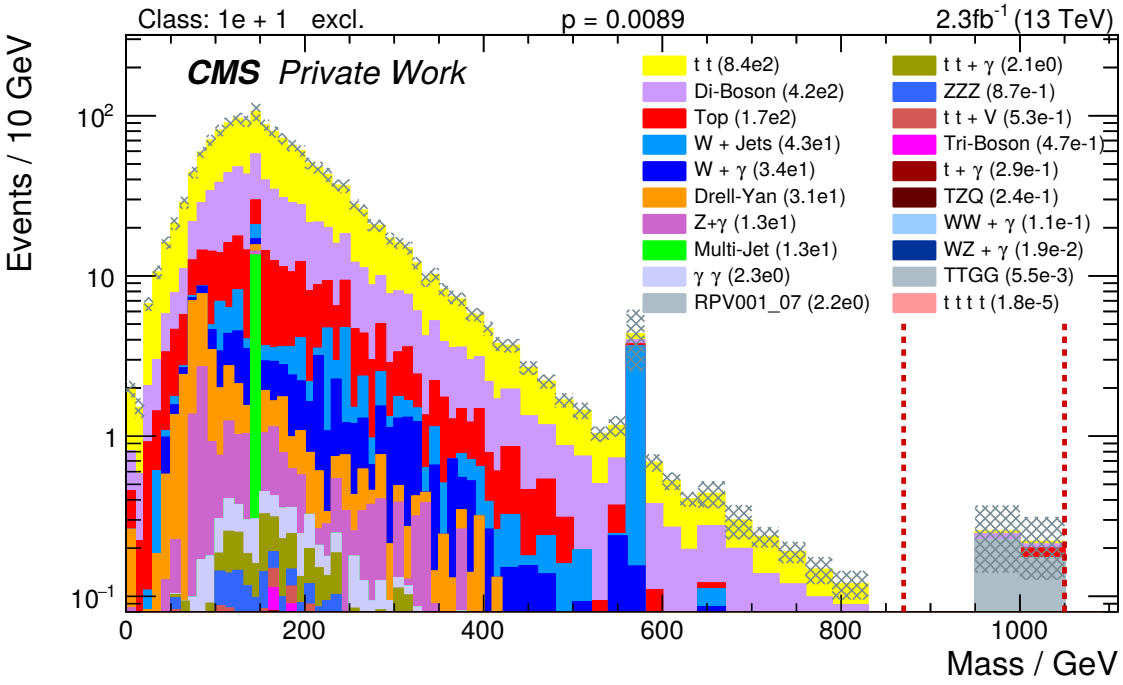

Figure 16: Invariant mass distribution of the exclusive event class $e + \mu$, $M_{\bar{\nu}_\tau} = 1000\,\text{GeV}$

7 Conclusion and Outlook

The analysis performed in this thesis has shown that MUSiC is principally sensitive to a model of the considered type. For the specific RPV theory the tau-sneutrino mass needs to be below a certain threshold to obtain a clear deviation in the $\tilde{p}$-plot and the deviation appears more and more clear with decreasing mass. All considered masses show a visible deviation, but it becomes clear that these deviations get smaller for increasing masses. As expected, the deviations become best visible in the invariant mass distribution and one of the most significant classes is $e + \mu$.

After future changes of MUSiC-programs one will be able to perform a similar study again and compare the results to the ones provided here in order to validate whether the sensitivity has changed. One might also consider models with different effects on the kinematic distributions (e.g. no resonant signal production). A further possibility to expand the workflow is to include even more sophisticated statistical methods to combine the results of the RoI-Scanner from all classes.
The further taking of data at the LHC will increase the recorded integrated luminosity of the CMS experiment so that the statistical uncertainties will continually decrease. An observation of a significant deviation from the Standard Model thus becomes more and more probable.

References

[1] Particle Data Group (PDG), *"Review of Particle Physics"*, 2014.
http://pdg.lbl.gov/2015/html/computer_read.html (Entire Book)

[2] PBS NOVA [1], Fermilab, Office of Science, United States Department of Energy, Particle Data Group, CC BY 3.0
https://commons.wikimedia.org/w/index.php?curid=4286964

[3] John Ellis, *"Limits of the Standard Model"*,
Lectures given at the PSI Summer School, 2002.
https://arxiv.org/abs/hep-ph/0211168

[4] John Ellis, *"Beyond the Standard Model for Hillwalkers"*,
Lectures presented at 1998 European School of High-Energy Physics, 1998.
http://arxiv.org/abs/hep-ph/9812235

[5] The Royal Swedish Academy of Sciences, *"Neutrino Oscillations"*,
Scientific Background on the Nobel Prize in Physics 2015, 2015.
https://www.nobelprize.org/nobel_prizes/physics/laureates/2015/advanced-physicsprize2015.pdf

[6] https://monttj.files.wordpress.com/2013/05/supersymmetry_zoom_new.jpg, 25.08.2016.

[7] Particle Data Group (PDG), *"Particle Physics Booklet"*, Page 150, 2014.
http://pdg.lbl.gov/2015/html/computer_read.html (Entire Booklet)

[8] Nobelprize.org, Nobel Media AB 2014, *"The 2004 Nobel Prize in Physics - Popular Information"*, Illustration by Typoform, Web. 25 Aug 2016.
https://www.nobelprize.org/nobel_prizes/physics/laureates/2004/popular.html

[9] S. Erdweg, A. Güth, T. Hebbeker, H. Keller, A. Meyer, S. Mukherjee, *"Search for lepton flavour violating decays of heavy resonances to eμ pairs in pp collisions at* $\sqrt{s}$=13 TeV *"*,
EXO-16-001, 2016.
http://cms.cern.ch/iCMS/analysisadmin/cadilines?line=EXO-16-001&tp=an&id=1566&ancode=EXO-16-001

[10] ALICE Collaboration, K Aamodt *et al.*, *"The ALICE experiment at the CERN LHC"*,
Journal of Instrumentation (Jinst), Volume 3, 2008.
http://iopscience.iop.org/article/10.1088/1748-0221/3/08/S08002/meta

[11] LHCb Collaboration, A Augusto Alves Jr *et al.*, *"The LHCb Detector at the LHC"*,
Journal of Instrumentation (Jinst), Volume 3, 2008.
http://iopscience.iop.org/article/10.1088/1748-0221/3/08/S08005/meta

[12] ATLAS Collaboration, G Aad *et al.*, *"The ATLAS Experiment at the CERN Large Hadron Collider"*,
Journal of Instrumentation (Jinst), Volume 3, 2008.
http://iopscience.iop.org/article/10.1088/1748-0221/3/08/S08003/meta

[13] CMS Collaboration, S Chatrchyan *et al.*, *"The CMS experiment at the CERN LHC"*,
Journal of Instrumentation (Jinst), Volume 3, 2008.
http://iopscience.iop.org/article/10.1088/1748-0221/3/08/S08004/meta

[14] P. Papacz, *"Model Unspecific Search for new Physics in CMS Based on 2011 Data"*.
PhD Thesis, RWTH Aachen, 2014.

[15] `http://www.teilchen.at/news/69`, 25.08.2016.

[16] D. Griffiths, *"Introduction to Elementary Particles"*, Weinheim: Wiley-VCH-Verlag,
2. revised edition, 2008.

[17] CERN, Photo by Maximilien Brice, Michael Hoch, Joseph Gobin, 2008.
`https://www.flickr.com/photos/arselectronica/5980280567`

[18] David Barney, PictureforPoint5oct04allparticles, CMS-doc-5582, 2011.
`https://cms-docdb.cern.ch/cgi-bin/PublicDocDB/ShowDocument?docid=5581`

[19] J. Roemer, *"Sensitivitätsstudie zur resonanten τ-Sneutrino-Produktion im eμ Endzustand mit CMS bei $\sqrt{s}$=13 TeV "*.
Bachelor Thesis, RWTH Aachen, 2014.
`https://web.physik.rwth-aachen.de/~hebbeker/theses/roemer_bachelor.pdf`

[20] J. Lieb, *"Development of a Fast Search Algorithm for the MUSiC Framework"*.
Bachelor Thesis, RWTH Aachen, 2015.
`https://web.physik.rwth-aachen.de/~hebbeker/theses/lieb_bachelor.pdf`

[21] H. Pieta, *"MUSiC - A Model Unspecific Search in CMS based on 2010 LHC data"*.
PhD Thesis, RWTH Aachen, 2012.
`https://web.physik.rwth-aachen.de/~hebbeker/theses/pieta_phd.pdf`

[22] M. Olschewski, *"Study of Alternative Statistical Methods for a Model Unspecific Search in CMS"*.
Diploma Thesis, RWTH Aachen, 2011.
`https://web.physik.rwth-aachen.de/~hebbeker/theses/olschewski_diploma.pdf`

[23] A. Albert, D. Duchardt, T. Hebbeker, S. Knutzen, A. Meyer, P. Papacz, T. Pook, *"MUSiC - A Model Unspecific Search for New Physics in pp Collisions at $\sqrt{s}$=8 TeV "*.
EXO-14-016, 2016.
`http://cms.cern.ch/iCMS/analysisadmin/cadilines?line=EXO-14-016&tp=an&id=1421&ancode=EXO-14-016`

[24] S. Schmitz, *"Model Unspecific Search for New Physics with High pT Photons in CMS"*.
Diploma Thesis, RWTH Aachen, 2009.
`https://web.physik.rwth-aachen.de/~hebbeker/theses/schmitz_diploma.pdf`

Appendix

A) List of used Signal Samples

RPVresonantToEMu_M-500_LLE_LQD-001_TuneCUETP8M1_13TeV-calchep-pythia8/RunIISpring16MiniAODv2-PUSpring16RAWAODSIM_reHLT_80X_mcRun2_asymptotic_v14-v1/MINIAODSIM

RPVresonantToEMu_M-700_LLE_LQD-001_TuneCUETP8M1_13TeV-calchep-pythia8/RunIISpring16MiniAODv2-PUSpring16RAWAODSIM_reHLT_80X_mcRun2_asymptotic_v14-v1/MINIAODSIM

RPVresonantToEMu_M-1000_LLE_LQD-001_TuneCUETP8M1_13TeV-calchep-pythia8/RunIISpring16MiniAODv2-PUSpring16RAWAODSIM_reHLT_80X_mcRun2_asymptotic_v14-v1/MINIAODSIM

B) Further p-tilde-plots with corresponding $\frac{\chi^2}{N}$

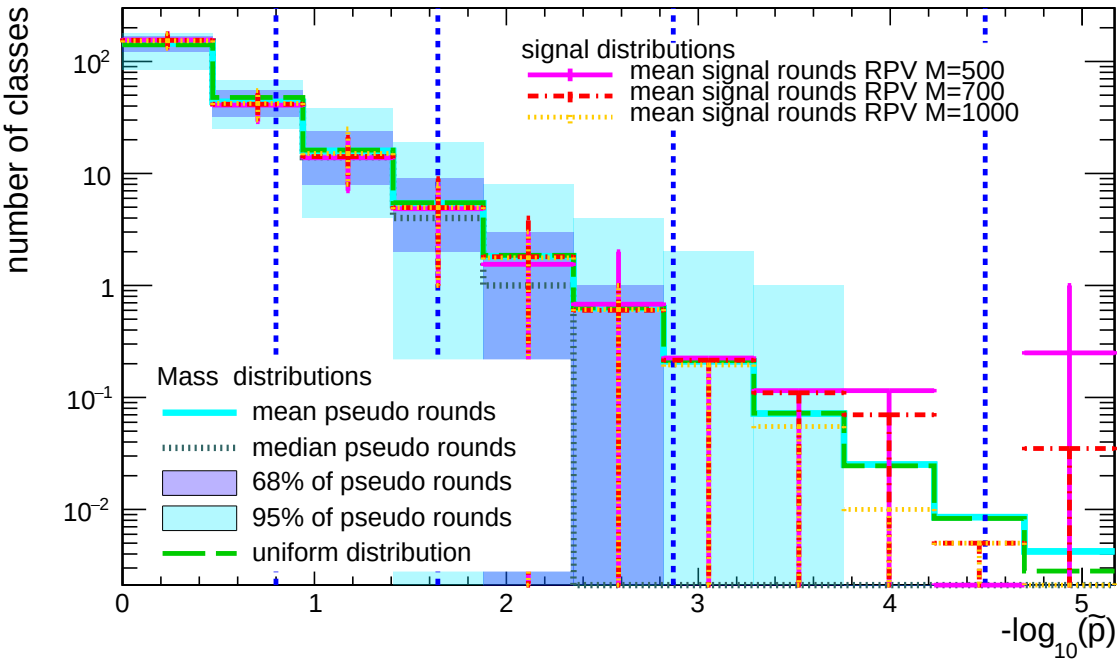

Figure 17: Mean, invariant Mass, inclusive variant

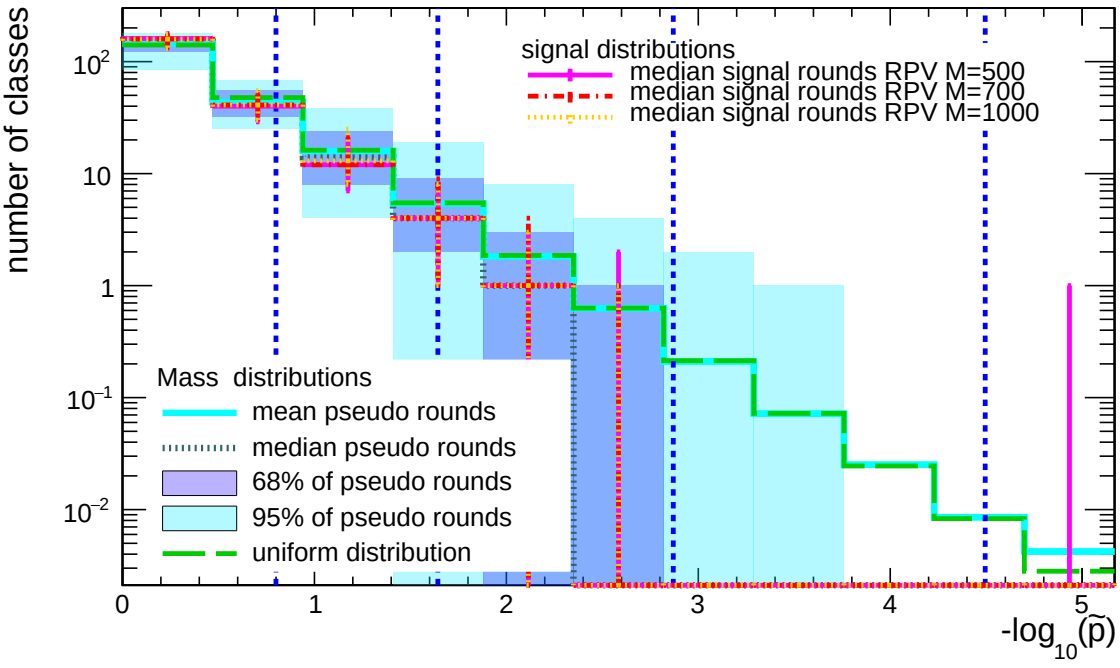

Figure 18: Median, invariant Mass, inclusive variant

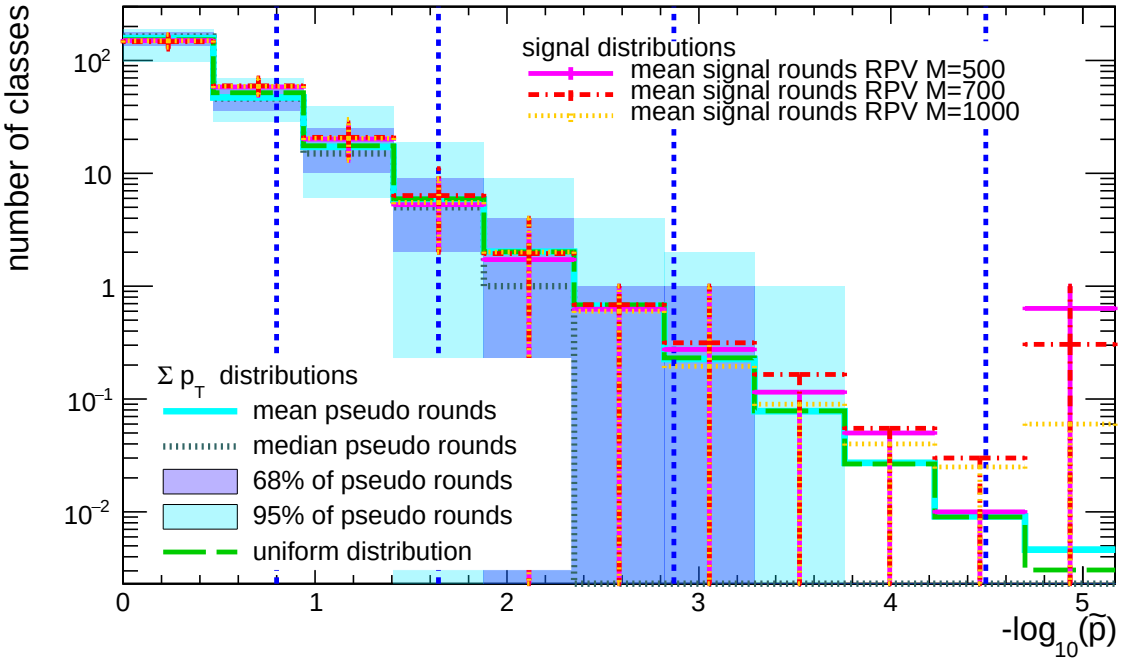

Figure 19: Mean, sum of transversal momenta, exclusive variant

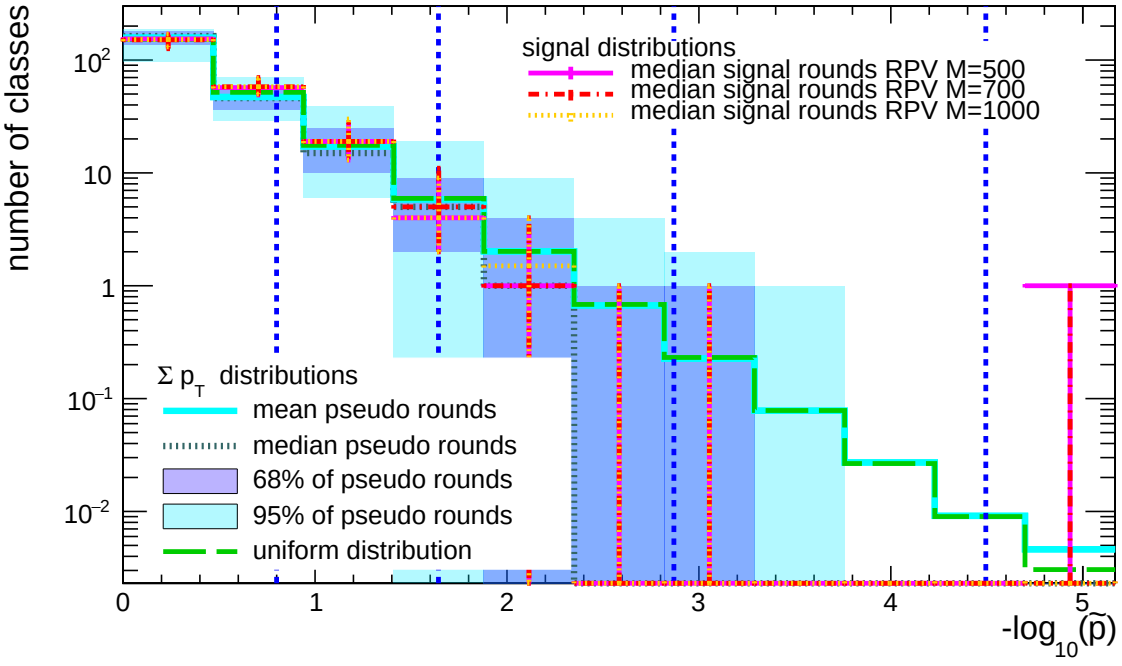

Figure 20: Median, sum of transversal momenta, exclusive variant

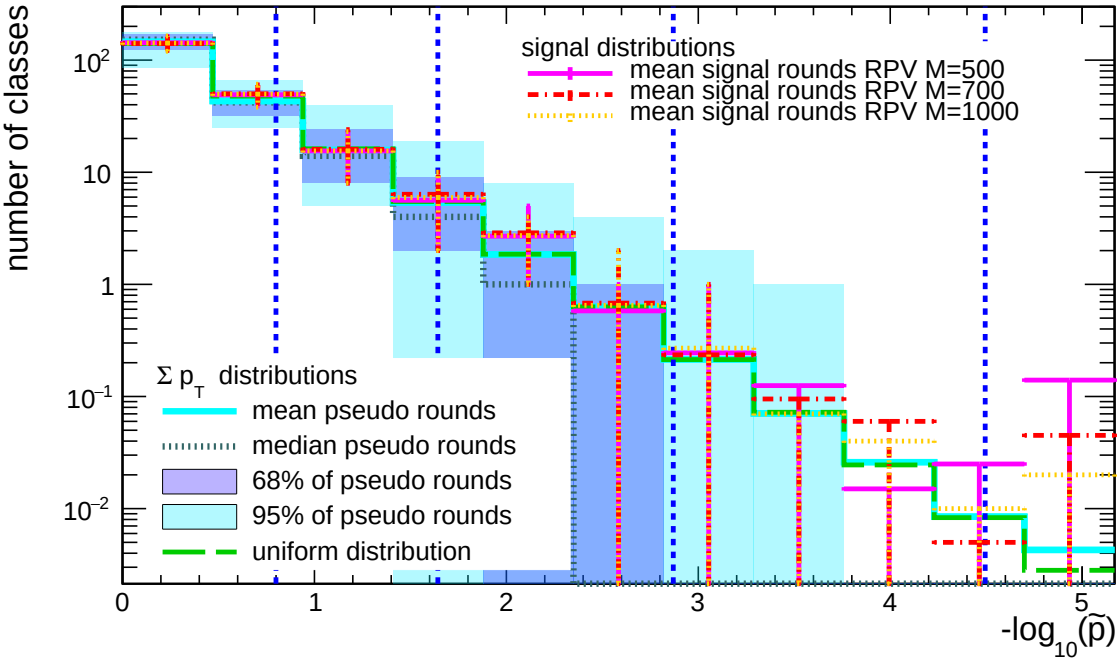

Figure 21: Mean, sum of transversal momenta, inclusive variant

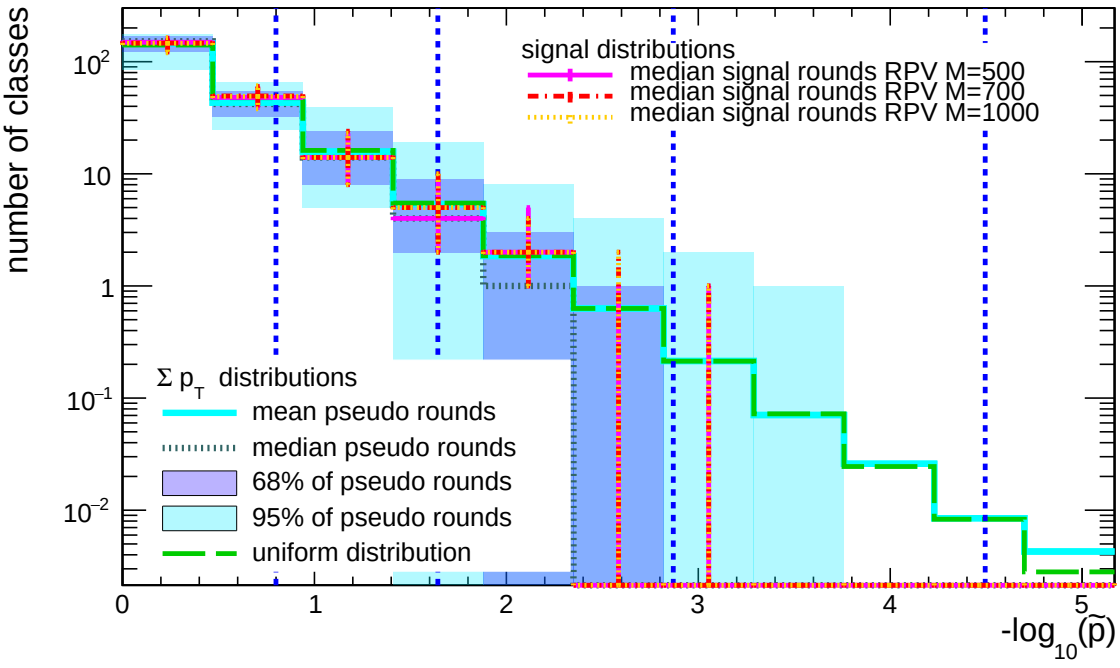

Figure 22: Median, sum of transversal momenta, inclusive variant

Table 4: $\frac{\chi^2}{N}$ for the mean with M_{inv} as kinematic variable and the inclusive variant

$M_{\tilde{\nu}_\tau}$	500 GeV	700 GeV	1000 GeV
$\frac{\chi^2}{N}$	0.349	0.305	0.308

Table 5: $\frac{\chi^2}{N}$ for the median with M_{inv} as kinematic variable and the inclusive variant

$M_{\tilde{\nu}_\tau}$	500 GeV	700 GeV	1000 GeV
$\frac{\chi^2}{N}$	0.047	0.032	0.024

Table 6: $\frac{\chi^2}{N}$ for the mean with $\sum p_T$ as kinematic variable and the exclusive variant

$M_{\tilde{\nu}_\tau}$	500 GeV	700 GeV	1000 GeV
$\frac{\chi^2}{N}$	0.583	0.764	0.601

Table 7: $\frac{\chi^2}{N}$ for the median with $\sum p_T$ as kinematic variable and the exclusive variant

$M_{\tilde{\nu}_\tau}$	500 GeV	700 GeV	1000 GeV
$\frac{\chi^2}{N}$	0.220	0.255	0.269

Table 8: $\frac{\chi^2}{N}$ for the mean with $\sum p_T$ as kinematic variable and the inclusive variant

$M_{\tilde{\nu}_\tau}$	500 GeV	700 GeV	1000 GeV
$\frac{\chi^2}{N}$	0.573	0.789	0.675

Table 9: $\frac{\chi^2}{N}$ for the median with $\sum p_T$ as kinematic variable and the inclusive variant

$M_{\tilde{\nu}_\tau}$	500 GeV	700 GeV	1000 GeV
$\frac{\chi^2}{N}$	0.127	0.175	0.167